Boron- and Nitrogen-Doped Graphene Quantum Dots/Graphene Hybrid Nanoplatelets as Efficient Electrocatalysts for Oxygen Reduction

Huilong Fei,[†] Ruquan Ye,[†] Gonglan Ye,[§] Yongji Gong,[†] Zhiwei Peng,[†] Xiujun Fan,[‡,∥] Errol L. G. Samuel,[†] Pulickel M. Ajayan,[*,†,§] and James M. Tour[*,†,‡,§]

[†]Department of Chemistry, [‡]Smalley Institute for Nanoscale Science and Technology, [§]Department of Materials Science and NanoEngineering, Rice University, 6100 Main Street, Houston, Texas 77005, United States and [∥]College of Electronic Information and Control Engineering, Beijing University of Technology, Beijing 100124, China

ABSTRACT The scarcity and high cost of platinum-based electrocatalysts for the oxygen reduction reaction (ORR) has limited the commercial and scalable use of fuel cells. Heteroatom-doped nanocarbon materials have been demonstrated to be efficient alternative catalysts for ORR. Here, graphene quantum dots, synthesized from inexpensive and earth-abundant anthracite coal, were self-assembled on graphene by hydrothermal treatment to form hybrid nanoplatelets that were then codoped with nitrogen and boron by high-temperature annealing. This hybrid material combined the advantages of both components, such as abundant edges and doping sites, high electrical conductivity, and high surface area, which makes the resulting materials excellent oxygen reduction electrocatalysts with activity even higher than that of commercial Pt/C in alkaline media.

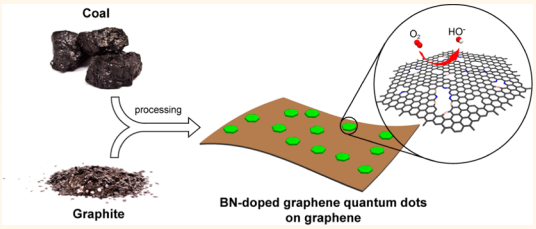

KEYWORDS: oxygen reduction reaction · electrocatalyst · boron nitrogen doping · graphene quantum dots · coal

The electrochemical performance of fuel cells is greatly affected by the oxygen reduction reaction (ORR) at the cathode because of its sluggish reaction kinetics.[1] To efficiently catalyze the ORR, platinum-loaded carbon is the most commonly used electrocatalyst. However, its large-scale production for commercial applications has been hindered by the high cost of Pt as well as by the time-dependent drift and CO deactivation problems of Pt-based electrodes.[2,3] Consequently, intensive research is underway to develop new ORR electrocatalyst alternatives to minimize or replace Pt; examples include Pt-based alloys,[4,5] inorganic/nanocarbon hybrid materials,[6] and heterocyclic polymers.[7] In particular, heteroatom (N, B, S, and P)-doped nanocarbon materials (carbon nanotubes, graphene, ordered mesoporous graphitic arrays, and carbon nanofibers) have attracted great interest due to their low-cost, high electrocatalytic activities, selectivity, and stability.[1,8−13] Further, it was found that co-doping carbon with two heteroatoms, B and N, can effectively create more catalytically active sites than singularly doped counterparts, resulting from synergistic coupling effects between heteroatoms.[14−16]

Recently, significant developments have been made on zero-dimensional graphene quantum dots (GQDs) associated with quantum-confinement and edge effects, leading to applications in photovoltaics, supercapacitors, bioimaging, and sensors.[17,18] The edge-abundant features of GQD are particularly advantageous for electrocatalysts as reactions are more readily electrochemically catalyzed at the edge planes than the basal plane.[19−21] Though nitrogen-doped GQDs have been demonstrated to be electrochemically active toward ORR,[22,23] the enhanced electrocatalytic activity is limited; this may be due to the low electrical conductivity of the electrode made using small GQD with high percolation threshold values, an important factor in determining the ORR electrocatalytic performance.

In spite of tremendous efforts in developing precious-metal-free and entirely metal-free ORR electrocatalysts, it still remains a challenge to develop efficient catalysts that

* Address correspondence to ajayan@rice.edu, tour@rice.edu.

Received for review August 18, 2014 and accepted September 24, 2014.

Published online September 24, 2014
10.1021/nn504637y

are comparable or even superior to commercial Pt/C. Here, we first synthesized graphene quantum dot/graphene (GQD/G) hybrid nanoplatelets by hydrothermal self-assembly and then codoped the GQD/G with boron and nitrogen to obtain BN-doped GQD/G(BN-GQD/G) hybrid nanoplatelets by annealing at high temperature for different time periods. The optimized samples show excellent ORR electrocatalytic activity with more positive onset potential than commercial Pt/C, and they also have large current densities.

RESULTS AND DISCUSSION

The preparation of BN-GQD/G is illustrated in Figure 1. The GQDs were synthesized through a facile and inexpensive method,[24] recently developed in our group, by oxidizing anthracite coal in H_2SO_4/HNO_3 acid (see Experimental Section for details). The GQDs were readily dispersible in water. A typical transmission electron microscopy (TEM) image of GQDs is shown in the Supporting Information (Figure S1) with a size of ~15−20 nm. The GQDs were mixed with an aqueous suspension of graphene oxide (GO) at a mass ratio of 2:1 and hydrothermally treated for 14 h. During the hydrothermal self-assembly process, GO with high surface area acted as a two-dimensional template to direct the assembly of GQDs; the strong interactions between the hydroxyl and carbonyl functional groups of GO and GQDs ensured the compact packing between them, leading to the formation of GQD/G hybrid nanoplatelets. After this self-assembly process, the mixture precipitated (Supporting Information Figure S2), indicating that the hydrothermal process reduced the GQDs and GO, rendering them insoluble and allowing efficient assembly between GQDs and GO. The morphology of the resulting GQD/G hybrid nanoplatelets was examined by scanning electron microscopy (SEM) and TEM. SEM images (Supporting Information Figure S3) clearly show the uniform flake-like structure with dimensions similar to the graphene sheets, but the surface observed from the higher magnification SEM image appears to be rougher when compared to that of graphene alone (Supporting Information Figure S4) due to the decoration of particle-like GQDs on the reduced GO sheets. The formation of the flake-like structure was further confirmed by TEM (Figure S5). The mass ratio of GQD to GO was found to be critical in the formation of flake-like structures. For example, when the GQD/GO ratio was decreased to 1:1, the flake-like structures were more graphene-like (Figure S6); however, when the ratio was increased to 3:1, severe aggregation took place (Figure S7) and no flake-like structures were observed. This is probably due to the insufficient surface area provided by GO to support the GQDs when the GQD amount is excessive. The GQD/G hybrid nanoplatelets were converted to BN-GQD/G by annealing at 1000 °C for different time periods using ammonia and boric acid as nitrogen and boron sources, respectively. The samples annealed for 10, 30, and 60 min are denoted as BN-GQD/G-10, BN-GQD/G-30, and BN-GQD/G-60, respectively. Boron- and nitrogen-codoped graphene (BN-G-30), nitrogen-doped GQD/G (N-GQD/G-30), and dopant-free (yet annealed) GQD/G (DF-GQD/G-30) were also prepared as control samples.

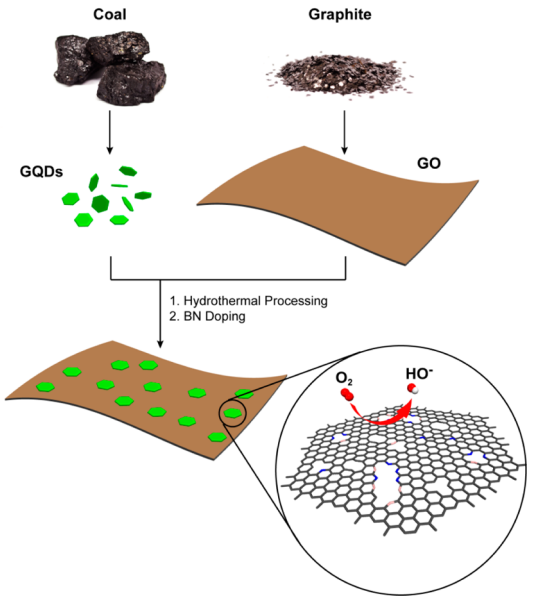

Figure 1. Illustration of the preparation procedure for the BN-GQD/G nanocomposite.

Figure 2a,b shows the SEM and low-magnification TEM images of BN-GQD/G-30; it can be seen that the flake-like structures were retained with no obvious aggregation after high-temperature treatment at 1000 °C. From high-magnification TEM (Figure 2c), small domains of defective graphitic structures were observed. The 2D features and thicknesses of the hybrid nanoplatelets were further characterized by AFM (Figure 2d), which revealed that the average thicknesses of the flakes were ~7 nm.

In the as-described architecture, graphene sheets not only behave as 2D platforms to allow the uniform distribution of GQDs but also, because of their higher electrical conductivity, they act as conductive substrates for efficient electron transfer to interconnect the GQDs. The GQDs are too small to provide a sufficient percolative network for good conductivity. In addition, the porous scaffold formed by the flake-like BN-GQD/G hybrid nanoplatelets allows facile transport of electrolyte and electro-reactants/products. More importantly, GQDs with their abundant exposed edges and oxygen-containing functional groups allow the easy incorporation of dopants, which are potential active sites for electrocatalytic reactions. These factors together suggest BN-GQD/G with good ORR performances as will be discussed later.

X-ray photoelectron spectroscopy (XPS) was used to determine the doping content and chemical state of

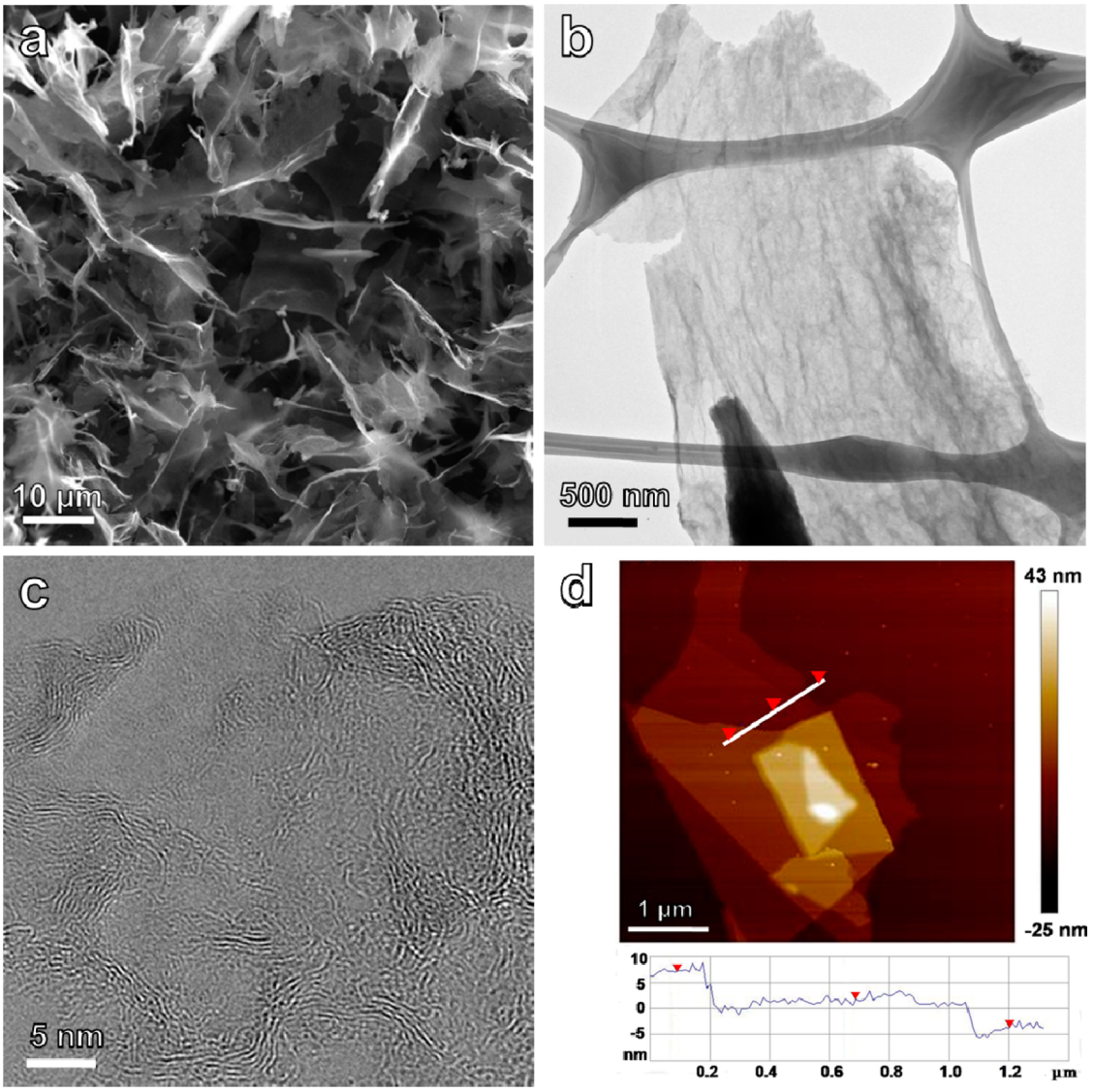

Figure 2. (a) SEM image of flake-like BN-GQD/G-30 nanoplatelets. (b) TEM image of a typical individual BN-GQD/G-30 nanoplatelet. (c) Higher magnification TEM image of BN-GQD/G-30. (d) AFM image of a partially stacked BN-GQD/G-30 nanoplatelet.

nitrogen and boron in the BN-GQD/G samples. Supporting Information Figure S8 shows the survey spectra of three BN-GQD/G samples with different doping times, along with BN-G-30, N-GQD/G-30, and dopant-free DF-GQD/G-30. In all of the BN-GQD/G samples, peaks characteristic of carbon, oxygen, boron, and nitrogen are present, and the peaks for boron and nitrogen become more pronounced as the doping time increases. This indicated that the BN doping process using boric acid and ammonia was effective, and the doping contents can be tuned by varying the doping time. For example, 30 min doping gave ~18.3 atom % nitrogen and ~13.6 atom % boron. In comparison, there was no boron in the N-GQD/G-30 sample, and both boron and nitrogen were absent in the DF-GQD/G-30. The chemical composition of these samples is summarized in Supporting Information Table S1. Figure 3 shows the high-resolution spectra of N 1s and B 1s for the BN-GQD/G samples. The N 1s spectra were deconvoluted into three peaks assignable to N−B bonding and pyridinic nitrogen (398.3 eV), pyrrolic nitrogen (399.8 eV), and quaternary nitrogen (401.1 eV).[16,25,26] The B 1s spectra were deconvoluted into two peaks with one peak at 191.0 eV for N−B−C moieties and another at 192.3 eV for BCO_2 species.[16] Careful analysis of the XPS data revealed that the N 1s and B 1s peaks are both dominated by N−B bonding species at 398.3 and 191.0 eV, respectively, and this dominance became more significant with the increase in doping time. This indicated that N and B tend to exist as pairs when the doping content was increased. The codoping of N and B and their concentration will be shown to have important roles in affecting the ORR electrocatalytic activities.

The ORR electrocatalytic properties were first examined by cyclic voltammetry (CV) in 0.1 M KOH solution

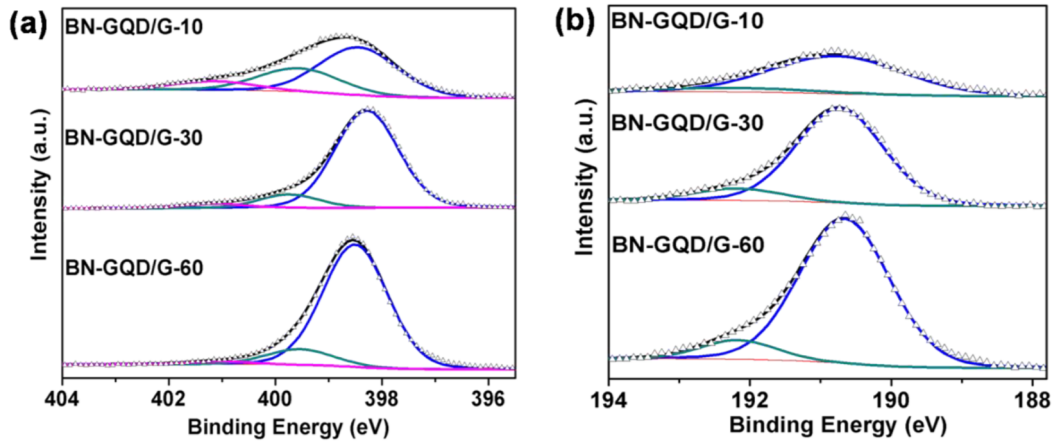

Figure 3. High-resolution (a) XPS N 1s and (b) XPS B 1s of BN-GQD/G-10, BN-GQD/G-30, and BN-GQD/G-60. All binding energies are referenced to C 1s at 284.5 eV.

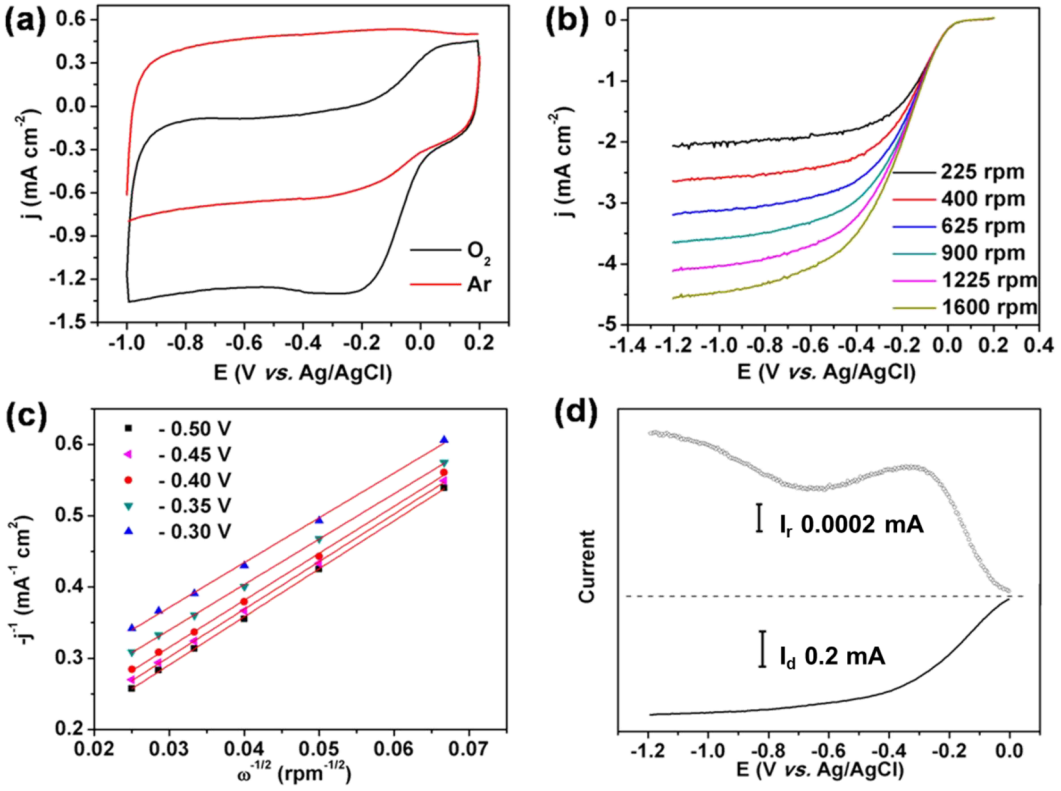

Figure 4. (a) Cyclic voltammograms of ORR on BN-GQD/G-30 in Ar- and O_2-saturated 0.1 M KOH solution at a scan rate of 100 mV s^{-1}. (b) RDE linear sweep voltammograms of ORR on a BN-GQD/G-30 electrode at different rotating speeds in O_2-saturated 0.1 M KOH solution with a scan rate of 5 mV s^{-1}. (c) Koutecky–Levich plots of BN-GQD/G-30 derived from RDE voltammograms in (b) at different potentials. (d) Rotating ring disk electrode voltammograms of ORR on a BN-GQD/G-30 electrode with a scan rate of 5 mV s^{-1}.

saturated with Ar or O_2 within the potential range from 0.2 to −1 V *vs* Ag/AgCl at the scan rate of 100 mV s^{-1}. Figure 4a shows the cyclic voltammograms for BN-GQD/G-30, and it can be seen that a featureless current response was observed in Ar-saturated solution with large double-layer charge capacitance due to its high surface area. In strong contrast, a distinct cathodic peak appeared with substantial increase in current density when the solution was saturated with O_2, indicating pronounced catalytic activity toward ORR. In addition, the onset potential of BN-GQD/G-30 determined from CV was comparable to Pt/C (Figure S9, both at ∼0 V).

To gain further insight into the ORR, rotating disk electrode (RDE) voltammetry was performed in O_2-saturated 0.1 M KOH aqueous solution with a scan rate of 5 mV s^{-1}. Figure 4b shows the RDE voltammograms for ORR of the BN-GQD/G-30 electrode at different rotating speeds. These data show typical increasing current densities with larger rotating speeds due to the shortened diffusion length at higher speeds.[27]

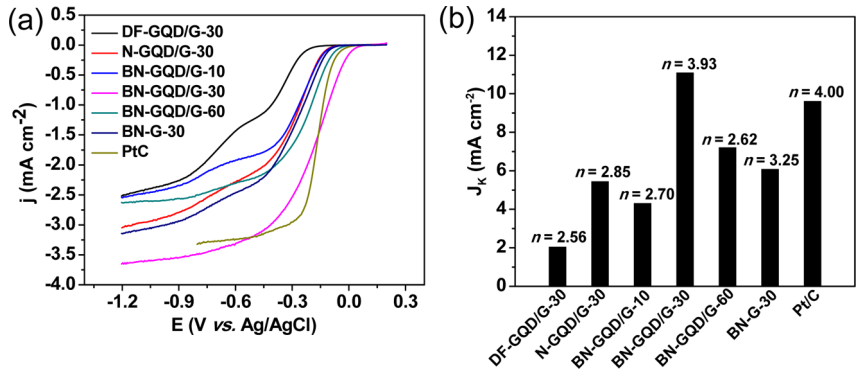

Figure 5. (a) RDE linear sweep voltammograms of ORR on DF-GQD/G-30, N-GQD/G-30, BN-GQD/G-10, BN-GQD/G-30, BN-GQD/G-60, BN-G-30, and Pt/C at a rotating speed of 900 rpm and scan rate of 5 mV s^{-1}. (b) Electrocatalytic activity given as the kinetic current density at −0.5 V for all samples in (a).

The kinetic parameters, including electron transfer numbers (*n*) and kinetic current density, were analyzed using the Koutecky−Levich (K−L) equations.[28] The linearity of the K−L plots (j^{-1} *vs* $\omega^{-1/2}$, Figure 4c) and near parallelism of the fitting lines indicated first-order kinetics toward the concentration of dissolved O_2 and similar *n* values at different potentials.[29] Remarkably, the average *n* for BN-GQD/G-30 hybrid nanoplatelets calculated from the slope of the K−L plots equals 3.93 in a potential range of −0.3 to −0.5 V (Figure 4c). This was further confirmed by a rotating ring disk electrode measurement that monitors the peroxide species (HO_2^-) produced during the ORR process.[30] The result (Figure 4d) shows that the ring current (I_r) was negligible compared to the disk current (I_d); the HO_2^- yield (Figure S10) was below ∼4% over the potential range from −0.2 to −0.12 V and gave an *n* of ∼3.95, suggesting a one-step, four-electron oxygen reduction pathway. In addition, the durability of the BN-GQD/G-30 was examined using the chronoamperometric technique. Continuous operation at −0.3 V gives a 73% current retention after 20 000 s (Figure S11), indicating its good stability in the alkaline medium. Cyclic and RDE voltammograms at different rotating speeds for the other samples (BN-GQD/G-10, BN-GQD/G-60, N-GQD/G-30, DF-GQD/G-30, BN-G-30, and commercial platinum on carbon black Pt/C) are in Figures S9 and S12.

Figure 5a shows the RDE voltammograms at 900 rpm for all samples. Except for the DF-GQD/G-30, which had a two-stage characterized ORR process, all other samples showed the typical one-stage processes, indicating the efficiency of incorporating dopants into the GQD/G hybrid nanoplatelets in enhancing ORR activity. Also, it was clear that the ORR activity was significantly influenced by doping time and the dopant concentration, with BN-GQD/G-30 having the most positive onset potential (0 V *vs* Ag/AgCl) and largest current density through the entire potential range. The relatively inferior ORR activities, less positive onset potentials, and smaller current densities of both BN-GQD/G-10 and BN-GQD/G-60 are supportive of the assertion that lower BN doping content results in a lower number of electrocatalytic sites. Likewise, higher BN doping content would produce B and N dopant pairs (as illustrated by the XPS analysis), which were found to be inactive toward ORR.[16] In addition, excessive B and N doping would decrease the electrical conductivity, as revealed by the impedance measurements (Figure S13),[28] which also contributes to the observed ORR activity degradation with the increase of doping time. To show the synergistic effects of dual B and N doping, N-GQD/G-30 was also included for comparison; it has a much more negative onset potential and smaller current density than BN-GQD/G-30 with the same doping time. To show the important role of GQD in improving ORR activity, BN-G-30 was tested and shows much inferior activity. When compared to commercial Pt/C, it is remarkable that the onset potential of BN-GQD/G-30 measured from the RDE voltammograms was ∼15 mV more positive than that of Pt/C. In addition, the diffusion-limited current density and current density in the potential range of 0.20 to −0.15 V of BN-GQD/G-30 was also larger than those of Pt/C at the same mass loading, suggesting the higher ORR activity of BN-GQD/G-30 than Pt/C. Figure 5b summarizes *n* and kinetic current densities (J_K) obtained from the K−L equation for all samples. BN-GQD/G-30 with its nearly full four-electron ORR process (*n* = 3.93) and large kinetic current (J_K = 11.1 mA cm^{-2}) outperformed DF-GQD/G-30 (*n* = 2.56, J_K = 2.1 mA cm^{-2}), N-GQD/G-30 (*n* = 2.62, J_K = 5.4 mA cm^{-2}), BN-G-30 (*n* = 3.25, J_K = 5.6 mA cm^{-2}), BN-GQD/G-10 (*n* = 2.70, J_K = 4.3 mA cm^{-2}), and BN-GQD/G-60 (*n* = 2.62, J_K = 7.2 mA cm^{-2}), highlighting the importance of tuning doping concentration and the synergistic codoping effects. More importantly, the kinetic current of BN-GQD/G-30 was even larger than that of Pt/C (J_K = 9.6 mA cm^{-2}).

CONCLUSION

In summary, with inexpensive and earth-abundant coal and graphite as raw materials, the low-cost production of boron- and nitrogen-codoped graphene

quantum dots/graphene hybrid nanoplatelets by hydrothermal reaction and postannealing treatment was demonstrated. With enriched edge and BN doping sites from graphene quantum dots and high electrical conductivity from graphene, the optimized hybrid nanoplatelets exhibit excellent ORR activity with ~15 mV more positive onset potential and similar current density when compared to commercial Pt/C.

EXPERIMENTAL SECTION

Synthesis of GO and GQD. GO was synthesized from graphite flakes (~150 μm flakes) using the improved Hummers method.[31] GQDs were synthesized from anthracite using our published procedure.[24] Briefly, 300 mg of anthracite coal (Fisher Scientific, catalogue number S98806) was suspended in concentrated H_2SO_4/HNO_3 (60 mL/20 mL) and then bath-sonicated (Cole Parmer, model 08849-00) for 2 h. The mixture was stirred and heated at 100 °C for 24 h. The reaction was allowed to cool to room temperature and poured into a beaker containing 100 mL of ice, followed by addition of NaOH (3 M) until the pH reached ~7. The obtained mixture was then filtered through a 0.45 μm polytetrafluoroethylene membrane, and the filtrate was dialyzed in a 1000 Da dialysis bag for 5 days.

Synthesis of GQD/GO Hybrid Nanoplatelets. GQD/GO hybrid nanoplatelets were prepared by a hydrothermal process. In a typical process, 20 mg of GQD and 10 mg of GO were added to 5 mL of DI water and bath-sonicated (Cole Parmer, model 08849-00) for 2 h to form a stable aqueous suspension. The resulting mixture was sealed in a Telfon-lined autoclave and hydrothermally treated at 180 °C for 14 h. Finally, the obtained samples were freeze-dried to obtain the powder product.

Synthesis of BN-GQD/GO. The BN doping process was performed using a CVD oven. Typically, GQD/GO was placed on a quartz boat in a standard 2.54 cm quartz tube furnace, and solid boric acid was placed in a lower temperature zone as a boron source. Then, the quartz tube was evacuated to ~100 mTorr, and Ar/NH_3 (300 sccm/30 sccm) was turned on as a nitrogen source. After that, the temperature was increased to 1000 °C within 30 min, and the reaction was allowed to proceed for another 10, 30, or 60 min to give BN-GQD/GO-10, BN-GQD/GO-30, or BN-GQD/GO-60, respectively. For comparison, DF-GQD/GO-30 and N-GQD/GO-30 were prepared using the same procedure with 30 min doping except no BN or B sources were provided, respectively. BN-G was prepared using the same procedure except no GQDs were added during the hydrothermal reaction.

Characterization. SEM was performed using FEI Quanta 400 high-resolution field emission scanning electron microscope in high-vacuum mode. TEM was performed using JEOL 2100 field emission gun transmission electron microscope. XPS spectra were taken on a PHI Quantera SXM scanning X-ray microprobe with a monochromatic 1486.7 eV Al Kα X-ray line source, 45° take off angle, and a 200 μm beam size. XPS spectra were taken on a PHI Quantera SXM scanning X-ray microprobe. Al anode at 25 W was used as an X-ray source with a pass energy of 26.00 eV, 45° take off angle, and a 100 μm beam size. A pass energy of 140 eV was used for survey and 26 eV for atomic concentration. Raman spectroscopy (Renishaw inVia) was performed at 514.5 nm laser excitation at a power of 20 mW.

Electrochemical Characterization. CV and RDE studies were conducted in a home-built electrochemical cell using a Ag/AgCl electrode as the reference electrode and a Pt wire as the counter electrode. For preparation of the electrode, BN-GQD/GO catalyst (2 mg) and 2 mL of 0.5 wt % Nafion aqueous solution were mixed and dispersed by sonication until a homogeneous ink was formed. Then, 16 μL of the catalyst ink was loaded onto a glassy carbon electrode (5 mm in diameter). The catalyst ink was dried slowly in air. A flow of O_2 was maintained in the electrolyte during the measurement to ensure continuous O_2 saturation. Commercial 20 wt % platinum on Vulcan carbon black (Pt/C from Alfa Aesa) was used for comparison, with all the testing parameters kept the same as that used for the BN-GQD/GO electrode.

Conflict of Interest: The authors declare no competing financial interest.

Acknowledgment. Support came from the ONR MURI program (#00006766, N00014-09-1-1066), the Air Force Office of Scientific Research (FA9550-09-1-0581), and the AFOSR MURI program (FA9550-12-1-0035). X. F. acknowledges the China Scholarship Council for partial support of this work.

Supporting Information Available: Additional SEM images, TEM images, XPS analyses, and electrochemical measurements. This material is available free of charge *via* the Internet at http://pubs.acs.org.

REFERENCES AND NOTES

1. Xiong, W.; Du, F.; Liu, Y.; Perez, A.; Supp, M.; Ramakrishnan, T. S.; Dai, L.; Jiang, L. 3-D Carbon Nanotube Structures Used as High Performance Catalyst for Oxygen Reduction Reaction. *J. Am. Chem. Soc.* **2010**, *132*, 15839–15841.
2. Debe, M. K. Electrocatalyst Approaches and Challenges for Automotive Fuel Cells. *Nature* **2012**, *486*, 43–51.
3. Arenz, M.; Mayrhofer, K. J. J.; Stamenkovic, V.; Blizanac, B. B.; Tomoyuki, T.; Ross, P. N.; Markovic, N. M. The Effect of the Particle Size on the Kinetics of CO Electrooxidation on High Surface Area Pt Catalysts. *J. Am. Chem. Soc.* **2005**, *127*, 6819–6829.
4. Hong, J. W.; Kang, S. W.; Choi, B. S.; Kim, D.; Lee, S. B.; Han, S. W. Controlled Synthesis of Pd–Pt Alloy Hollow Nanostructures with Enhanced Catalytic Activities for Oxygen Reduction. *ACS Nano* **2012**, *6*, 2410–2419.
5. Hwang, S. J.; Kim, S. K.; Lee, J. G.; Lee, S. C.; Jang, J. H.; Kim, P.; Lim, T. H.; Sung, Y. E.; Yoo, S. J. Role of Electronic Perturbation in Stability and Activity of Pt-Based Alloy Nanocatalysts for Oxygen Reduction. *J. Am. Chem. Soc.* **2012**, *134*, 19508–19511.
6. Liang, Y.; Li, Y.; Wang, H.; Dai, H. Strongly Coupled Inorganic/Nanocarbon Hybrid Materials for Advanced Electrocatalysis. *J. Am. Chem. Soc.* **2013**, *135*, 2013–2036.
7. Winther-Jensen, B.; Winther-Jensen, O.; Forsyth, M.; MacFarlane, D. R. High Rates of Oxygen Reduction over a Vapor Phase-Polymerized PEDOT Electrode. *Science* **2008**, *321*, 671–674.
8. Wang, Z.; Jia, R.; Zheng, J.; Zhao, J.; Li, L.; Song, J.; Zhu, Z. Nitrogen-Promoted Self-Assembly of N-Doped Carbon Nanotubes and Their Intrinsic Catalysis for Oxygen Reduction in Fuel Cells. *ACS Nano* **2011**, *5*, 1677–1684.
9. Dai, L. Functionalization of Graphene for Efficient Energy Conversion and Storage. *Acc. Chem. Res.* **2012**, *46*, 31–42.
10. Fellinger, T. P.; Hasché, F.; Strasser, P.; Antonietti, M. Mesoporous Nitrogen-Doped Carbon for the Electrocatalytic Synthesis of Hydrogen Peroxide. *J. Am. Chem. Soc.* **2012**, *134*, 4072–4075.
11. Bo, X.; Guo, L. Ordered Mesoporous Boron-Doped Carbons as Metal-Free Electrocatalysts for the Oxygen Reduction Reaction in Alkaline Solution. *Phys. Chem. Chem. Phys.* **2013**, *15*, 2459–2465.
12. Tang, Y.; Allen, B. L.; Kauffman, D. R.; Star, A. Electrocatalytic Activity of Nitrogen-Doped Carbon Nanotube Cups. *J. Am. Chem. Soc.* **2009**, *131*, 13200–13201.
13. Maldonado, S.; Stevenson, K. J. Influence of Nitrogen Doping on Oxygen Reduction Electrocatalysis at Carbon Nanofiber Electrodes. *J. Phys. Chem. B* **2005**, *109*, 4707–4716.
14. Zheng, Y.; Jiao, Y.; Ge, Y.; Jaroniec, M.; Qiao, S. Z. Two-Step Boron and Nitrogen Doping in Graphene for Enhanced Synergistic Catalysis. *Angew. Chem.* **2013**, *125*, 3192–3198.
15. Wang, S.; Iyyamperumal, E.; Roy, A.; Xue, Y.; Yu, D.; Dai, L. Vertically Aligned BCN Nanotubes as Efficient Metal-Free Electrocatalysts for the Oxygen Reduction Reaction: A Synergetic Effect by Co-doping with Boron and Nitrogen. *Angew. Chem., Int. Ed.* **2011**, *50*, 11756–11760.

16. Zhao, Y.; Yang, L.; Chen, S.; Wang, X.; Ma, Y.; Wu, Q.; Jiang, Y.; Qian, W.; Hu, Z. Can Boron and Nitrogen Co-doping Improve Oxygen Reduction Reaction Activity of Carbon Nanotubes. *J. Am. Chem. Soc.* **2013**, *135*, 1201–1204.
17. Zhang, Z.; Zhang, J.; Chen, N.; Qu, L. Graphene Quantum Dots: An Emerging Material for Energy-Related Applications and Beyond. *Energy Environ. Sci.* **2012**, *5*, 8869–8890.
18. Shen, J.; Zhu, Y.; Yang, X.; Li, C. Graphene Quantum Dots: Emergent Nanolights for Bioimaging, Sensors, Catalysis and Photovoltaic Devices. *Chem. Commun.* **2012**, *48*, 3686–3699.
19. Kim, H.; Lee, K.; Woo, S. I.; Jung, Y. On the Mechanism of Enhanced Oxygen Reduction Reaction in Nitrogen-Doped Graphene Nanoribbons. *Phys. Chem. Chem. Phys.* **2011**, *13*, 17505–17510.
20. Yu, Y.; Nagelli, E.; Du, F.; Dai, L. Metal-Free Carbon Nanomaterials Become More Active than Metal Catalysts and Last Longer. *J. Phys. Chem. Lett.* **2010**, *1*, 2165–2173.
21. Xing, T.; Zheng, Y.; Li, L.; Cowie, B. C. C.; Gunzelmann, D.; Qiao, S.; Huang, S.; Chen, Y. Observation of Active Sites for Oxygen Reduction Reaction on Nitrogen-Doped Multilayer Graphene. *ACS Nano* **2014**, *8*, 6856–6862.
22. Li, Y.; Zhao, H.; Cheng, Y.; Hu, G.; Shi, L.; Dai, L.; Qu, L. Nitrogen-Doped Graphene Quantum Dots with Oxygen-Rich Functional Groups. *J. Am. Chem. Soc.* **2012**, *134*, 15–18.
23. Li, Q.; Zhang, S.; Dai, L.; Li, L. Nitrogen-Doped Colloidal Graphene Quantum Dots and Their Size-Dependent Electrocatalytic Activity for the Oxygen Reduction Reaction. *J. Am. Chem. Soc.* **2012**, *134*, 18932–18935.
24. Ye, R.; Xiang, C.; Lin, J.; Peng, Z.; Huang, K.; Yan, Z.; Cook, N. P.; Samuel, E. L. G.; Hwang, C.; Ruan, G.; Ceriotti, G.; Raji, A. O.; Marti, A. A.; Tour, J. M. Coal as an Abundant Source of Graphene Quantum Dots. *Nat. Commun.* **2013**, *4*, 2943.
25. Wang, H.; Maiyalagan, T.; Wang, X. Review on Recent Progress in Nitrogen-Doped Graphene: Synthesis, Characterization, and Its Potential Applications. *ACS Catal.* **2012**, *2*, 781–794.
26. Choi, C.; Park, S.; Woo, S. Binary and Ternary Doping of Nitrogen, Boron, and Phosphorus into Carbon for Enhancing Electrochemical Oxygen Reduction Activity. *ACS Nano* **2012**, *6*, 7084–7091.
27. Tan, Y.; Xu, C.; Chen, G.; Fang, X.; Zheng, N.; Xie, Q. Facile Synthesis of Manganese-Oxide-Containing Mesoporous Nitrogen-Doped Carbon for Efficient Oxygen Reduction. *Adv. Funct. Mater.* **2012**, *22*, 4584–4591.
28. Yang, S.; Feng, X.; Wang, X.; Müllen, K. Graphene-Based Carbon Nitride Nanosheets as Efficient Metal-Free Electrocatalysts for Oxygen Reduction Reactions. *Angew. Chem., Int. Ed.* **2011**, *50*, 5339–5343.
29. Liang, Y.; Li, Y.; Wang, H.; Zhou, J.; Wang, J.; Regier, T.; Dai, H. Co_3O_4 Nanocrystals on Graphene as a Synergistic Catalyst for Oxygen Reduction Reaction. *Nat. Mater.* **2011**, *10*, 780–786.
30. Paulus, U. A.; Schmidt, T. J.; Gasteiger, H. A.; Behm, R. J. Oxygen Reduction on a High-Surface Area Pt/Vulcan Carbon Catalyst: A Thin-Film Rotating Ring-Disk Electrode Study. *J. Electroanal. Chem.* **2001**, *495*, 134–135.
31. Marcano, D. C.; Kosynkin, D. V.; Berlin, J. M.; Sinitskii, A.; Sun, Z.; Slesarev, A.; Alemany, L. B.; Lu, W.; Tour, J. M. Improved Synthesis of Graphene Oxide. *ACS Nano* **2010**, *4*, 4806–4814.